PROCEEDINGS OF THE ROYAL SOCIETY B BIOLOGICAL SCIENCES

The Assembly of Ionic Currents in a Thalamic Neuron I. The Three-Dimensional Model

R. M. Rose and J. L. Hindmarsh

Proc. R. Soc. Lond. B 1989 **237**, 267-288
doi: 10.1098/rspb.1989.0049

Proc. R. Soc. Lond. B **237**, 267–288 (1989)
Printed in Great Britain

The assembly of ionic currents in a thalamic neuron I. The three-dimensional model

By R. M. Rose[1] and J. L. Hindmarsh[2]

[1] *Department of Physiology and* [2] *School of Mathematics, University of Wales College of Cardiff, Cardiff CF1 1SS, U.K.*

(*Communicated by Sir Andrew Huxley, F.R.S. – Received* 24 *August* 1988 – *Revised* 24 *February* 1989)

[Plate 1]

We have previously discussed qualitative models for bursting and thalamic neurons that were obtained by modifying a simple two-dimensional model for repetitive firing. In this paper we report the results of making a similar sequence of modifications to a more elaborate six-dimensional model of repetitive firing which is based on the Hodgkin–Huxley equations. To do this we first reduce the six-dimensional model to a two-dimensional model that resembles our original two-dimensional qualitative model. This is achieved by defining a new variable, which we call q. We then add a subthreshold inward current and a subthreshold outward current having a variable, z, that changes slowly. This gives a three-dimensional (v, q, z) model of the Hodgkin–Huxley type, which we refer to as the z-model. Depending on the choice of parameter values this model resembles our previous models of bursting and thalamic neurons. At each stage in the development of these models we return to the corresponding seven-dimensional model to confirm that we can obtain similar solutions by using the complete system of equations.

The analysis of the three-dimensional model involves a state diagram and a stability diagram. The state diagram shows the projection of the phase path from v, q, z space into the v, z plane, together with the projections of the curves $\dot{z} = 0$ and $\dot{v} = \dot{q} = 0$. The stability of the points on the curve $\dot{v} = \dot{q} = 0$, which we call the v, q nullcurve, is determined by the stability diagram. Taken together the state and stability diagrams show how to assemble the ionic currents to produce a given firing pattern.

Introduction

We have recently discussed a series of qualitative models of repetitive firing (Hindmarsh & Rose 1982), burst generation (Hindmarsh & Rose 1984), and of a thalamic neuron (Rose & Hindmarsh 1985), which were based on the model of Fitzhugh (1961). The repetitive firing model was given by the equations

$$\left.\begin{aligned} x &= y - F(x) + I, \\ y &= G(x) - y, \end{aligned}\right\} \tag{1}$$

where I is the applied current, $G(x)$ is a quadratic, and $F(x)$ is a cubic function. The

most important property of these equations is that the nullclines are in close proximity for $x < 0$, forming what we have called a 'narrow channel' in the x, y phase plane. This narrow channel property is of crucial importance to our theory for two reasons. First, it provides an explanation of the long inter-spike interval of neurons. This comes about because the limit cycle enters the narrow channel where the phase point is close to both nullclines, and so both $\dot{x}$ and $\dot{y}$ are small resulting in a slow change in the state of the system. Secondly, the closeness of the nullclines suggested the creation of additional equilibrium points (EPS) by a small deformation of one of them. One such deformation gave our bursting model (Hindmarsh & Rose 1984) which has two additional EPS. A second deformation in this narrow channel region gave our model of a thalamic neuron (Rose & Hindmarsh 1985), which has five EPS.

It can be seen that these models paid particular attention to the behaviour of the cell in the subthreshold region. To obtain the bursting and thalamic models it was necessary to add a third differential equation to equation (1), to represent a slow adaptation variable, giving the equations

$$\left.\begin{aligned} \dot{x} &= y - F(x) + I - z, \\ \dot{y} &= G(x) - y, \\ \dot{z} &= \tau^{-1}[H(x) - z], \end{aligned}\right\} \tag{2}$$

here $H(x)$ is a linear function and τ is a large time constant.

These models, although qualitative, are not entirely unrealistic. One possible interpretation of the deformations in the subthreshold region and the z variable is that they correspond to inward currents and a slow outward current respectively. We aim to replace these earlier qualitative models by models with ionic currents.

To begin with, consider the Hodgkin–Huxley equations for the squid axon (Hodgkin & Huxley 1952):

$$\left.\begin{aligned} \dot{v} &= C^{-1}[-g_{\mathrm{Na}} m^3 h (v - v_{\mathrm{Na}}) - g_{\mathrm{K}} n^4 (v - v_{\mathrm{K}}) - g_L (v - v_L) + I] \\ \dot{m} &= \tau_m^{-1}(v)\,[m_\infty(v) - m] \\ \dot{h} &= \tau_h^{-1}(v)\,[h_\infty(v) - h] \\ \dot{n} &= \tau_n^{-1}(v)\,[n_\infty(v) - n] \end{aligned}\right\} \tag{3}$$

where C, v_{Na}, v_{K}, v_L, g_{Na}, g_{K} and g_L are constants, and I is the externally applied current.

To understand this four-dimensional system of equations there have been several attempts to approximate it by simpler systems of lower dimension (Krinskii & Kokoz 1973; Kokoz & Krinskii 1973; Plant 1976; Rinzel 1978). There are two approximations. The first depends on the fact that because τ_m is small, m remains close to $m_\infty(v)$. Thus m is replaced by $m_\infty(v)$. The second is based on the observation that for the Hodgkin–Huxley equations the variables n and h are approximately related by $n + h = G$ (constant). Thus h is replaced by $G - n$.

Elimination of m and h leaves the following two-dimensional system derived by Krinskii & Kokoz (1973):

$$\left.\begin{aligned}\dot{v} &= C^{-1}[-g_{\mathrm{Na}}\, m_\infty^3(v)\,(G-n)\,(v-v_{\mathrm{Na}})-g_{\mathrm{K}}\, n^4(v-v_{\mathrm{K}})-g_L(v-v_L)+I],\\ \dot{n} &= \tau_n^{-1}(v)\,[n_\infty(v)-n].\end{aligned}\right\} \tag{4}$$

The nullclines for this equation are given by $\dot{v}=0$ where

$$-g_{\mathrm{Na}}\, m_\infty^3(v)\,(G-n)\,(v-v_{\mathrm{Na}})-g_{\mathrm{K}}\, n^4(v-v_{\mathrm{K}})-g_L(v-v_L)+I=0$$

and $\dot{n}=0$ where $n_\infty(v)-n=0$.

Although the nullclines of the Kokoz–Krinskii model are similar to those of our repetitive firing model (Hindmarsh & Rose 1982), the most significant point is that the narrow channel property is not present. In the subthreshold region of the v,n plane there is a wide gap between the nullclines however the parameters are chosen (Kokoz & Krinskii 1973). Therefore, our x and y variables cannot correspond to the v and n variables in the Hodgkin–Huxley equations, and Kokoz & Krinskii's analysis would appear to cast some doubt on the validity of our equations.

The way out of this difficulty came when we realized that the inter-spike interval for squid-axon repetitive firing is relatively short. For instance, the spike : inter-spike interval ratio for the lowest stimulating currents is of the order of 1 : 10 in the squid axon, yet our model for repetitive firing can give ratios of the order of 1 : 100. This suggests that our generalized model may be more relevant to neurons that fire at low frequency, and that Kokoz & Krinskii's analysis applies to higher-frequency firing. Therefore our equations may not apply to the squid axon, but may apply to neurons possessing an additional ionic current that results in low frequency firing. It is known that low-frequency firing is often associated with the presence of a fast transient outward current (I_A). This A-current was originally described in molluscan neurons (see Hagiwara *et al.* 1961 ; Connor & Stevens 1971 ; Neher 1971), and has now been found in many other neurons (Rogawski 1985). These considerations suggested that we should try to represent the firing of a cell with an A-current by a two-dimensional system and try to choose variables that would give nullclines similar to those of our original repetitive-firing model (Hindmarsh & Rose 1982). We begin by considering this problem.

Repetitive firing

The first quantitative description of the role of the fast transient outward current in repetitive firing was given by Connor & Stevens (1971) for a molluscan neuron, and this model was later extended to the crab axon by Connor *et al.* (1977). We have chosen the crab axon equations for our analysis because Connor *et al.* (1977) started with the original Hodgkin–Huxley equations (equation (3)). They added a term $g_A\, a^3 b(v-v_A)$ to the equation for $\dot{v}$, where a is the activation variable and b the inactivation variable of the A-current. We have also added this term,

except that to simplify the equations we have replaced $v_A = -75$ mV by $v_K = -72$ mV. This gives the following sixth-order system:

$$\left.\begin{aligned}
\dot{v} &= C^{-1}\{-g_{Na}\, m^3 h(v-v_{Na}) - g_L(v-v_L) - g_K\, n^4(v-v_K) - g_A\, a^3 b(v-v_K) + I\},\\
\dot{m} &= \tau_m^{-1}(v)\,[m_\infty(v) - m],\\
\dot{h} &= \tau_h^{-1}(v)\,[h_\infty(v) - h],\\
\dot{n} &= \tau_n^{-1}(v)\,[n_\infty(v) - n],\\
\dot{a} &= \tau_a^{-1}(v)\,[a_\infty(v) - a],\\
\dot{b} &= \tau_b^{-1}(v)\,[b_\infty(v) - b].
\end{aligned}\right\} \quad (5)$$

In this equation most of the parameters are the same as those of the Hodgkin–Huxley equations except that τ_m, τ_h, and τ_n have been scaled to a temperature of 18 °C, and m_∞, h_∞ and n_∞ have each been shifted along the voltage axis to give a reasonable fit to the crab voltage-clamp data. The exact modifications to the Hodgkin–Huxley equations together with the definitions of a_∞, b_∞, τ_a and τ_b are given by Connor *et al.* (1977) and have been restated in Appendix A as they form the basis of our analysis. We shall now approximate equation (5) by simpler systems in two and three dimensions.

First, we eliminate the m variable by arguing that because the time constant τ_m is small, $m(t) \approx m_\infty(v(t))$. Thus we ignore the equation for $\dot{m}$ and replace the m variable in the equation for $\dot{v}$ by $m_\infty(v)$, so that the equation for $\dot{v}$ becomes

$$\dot{v} = C^{-1}\{-g_{Na}\, m_\infty^3(v)\, h(v-v_{Na}) - g_L(v-v_L) - g_K[n^4 + (g_A/g_K)\, a^3 b]\,(v-v_K) + I\}.$$

Next note that although the term $n^4 + (g_A/g_K)\, a^3 b$ involves three variables, we may ignore the variation in a^3 because numerical integration of equation (5) shows that during recovery, when n^4 is insignificant, a^3 is approximately constant with value 0.21, and during action the terms $(g_A/g_K)\, a^3 b$ and $(g_A/g_K)\ 0.21 b$ are insignificant compared with n^4. We now replace the n variable and its differential equation by putting $w = n^4$ so that

$$\left.\begin{aligned}
\dot{w} = 4n^3\dot{n} &= 4n^3\,\tau_n^{-1}(v)\,[n_\infty(v) - n],\\
&= \tau_n^{-1}(v)\,[4n^3 n_\infty(v) - 3n^4 - n^4],\\
&= \tau_n^{-1}(v)\,\{n^3[4n_\infty(v) - 3n] - n^4\}.
\end{aligned}\right\} \quad (6)$$

Now although the n in equation (6) should be replaced by $w^{\frac{1}{4}}$, a much simpler equation is obtained if we replace n by $n_\infty(v)$ to get

$$\dot{w} = \tau_n^{-1}(v)\,[n_\infty^4(v) - w]. \quad (7)$$

Under voltage-clamp conditions the equilibrium value of w is the same for both equation (6) and equation (7), but the approach to equilibrium is slightly different.

Now define a new variable q by $q = w + Ab$, where $A = 0.21$ (g_A/g_K). This is done because the resulting equations closely resemble those of our earlier model (Hindmarsh & Rose 1982). Note that q is a conductance variable, and $g_K q$ is the sum of the conductances of the A and K currents. Because $\tau_b(v) \approx \tau_n(v)$ (figure 1*c*),

we replace both τ_b and τ_n by the average value $\tau_q(v) = 0.5\,[\tau_b(v)+\tau_n(v)]$. It now follows that

$$\begin{aligned}\dot{q} &= \dot{w}+A\dot{b},\\ &= \tau_q^{-1}(v)\,[n_\infty^4(v)-w]+\tau_q^{-1}(v)\,[Ab_\infty(v)-Ab],\\ &= \tau_q^{-1}(v)\,[n_\infty^4(v)+Ab_\infty(v)-(w+Ab)],\\ &= \tau_q^{-1}(v)\,[q_\infty(v)-q],\end{aligned}$$

where $$q_\infty(v) = n_\infty^4(v)+Ab_\infty(v).$$

Numerical integration of equations (5) shows that during both action and recovery $h(t) \approx -3n^4(t)+0.85$ so that we replace the variable h by $-3(q-Ab)+0.85$. Note that in principle $h(t)$ can now vary between -2.15 and 0.85. However, in practice $h(t)$ rarely leaves the physical range of 0 to 1.

We are now left with the following system of three differential equations:

$$\left.\begin{aligned}\dot{v} &= C^{-1}\{-g_{\mathrm{Na}}\,m_\infty^3(v)\,[-3(q-Ab)+0.85]\,(v-v_{\mathrm{Na}})-g_L(v-v_L)-g_{\mathrm{K}}\,q(v-v_{\mathrm{K}})+I\},\\ \dot{q} &= \tau_q^{-1}(v)\,[q_\infty(v)-q],\\ \dot{b} &= \tau_b^{-1}(v)\,[b_\infty(v)-b].\end{aligned}\right\} \tag{8}$$

Numerical integration of these equations shows that $b(t) \approx b_\infty[v(t)]$ for most of the firing cycle. This is also true for the complete equation (5) and happens because $b_\infty(v)$ only changes significantly with v in the subthreshold region where v is changing slowly with time. This slow change allows $b(t)$ to stay close to $b_\infty[v(t)]$. Therefore a further approximation can be made by ignoring the $\dot{b}$ equation and replacing b in the $\dot{v}$ equation by $b_\infty(v)$. This gives the following two-dimensional system:

$$\left.\begin{aligned}\dot{v} &= C^{-1}[-g_{\mathrm{Na}}\,m_\infty^3(v)\,\{-3[q-Ab_\infty(v)]+0.85\}\,(v-v_{\mathrm{Na}})-g_L(v-v_L)-g_{\mathrm{K}}\,q(v-v_{\mathrm{K}})+I],\\ \dot{q} &= \tau_q^{-1}(v)\,[q_\infty(v)-q].\end{aligned}\right\} \tag{9}$$

In figure 1*a* the numerical solution of these equations is compared with that of the sixth-order system (equation (5)). To match the inter-spike intervals, slightly different values of the external current, I, were chosen in the two cases.

The nullclines for equation (9) are given by:

$$\dot{v} = 0$$

when $$q = \frac{g_{\mathrm{Na}}[3Ab_\infty(v)+0.85]\,m_\infty^3(v)\,(v-v_{\mathrm{Na}})+g_L(v-v_L)-I}{3g_{\mathrm{Na}}\,m_\infty^3(v)\,(v-v_{\mathrm{Na}})-g_{\mathrm{K}}(v-v_{\mathrm{K}})}$$

and $\dot{q} = 0$ when $q = q_\infty(v)$.

In the v, q phase plane (figure 1*b*) we see that the v and q nullclines lie in close proximity, forming a narrow channel similar to that of our original repetitive firing model (Hindmarsh & Rose 1982). Note that if we had retained the n variable and

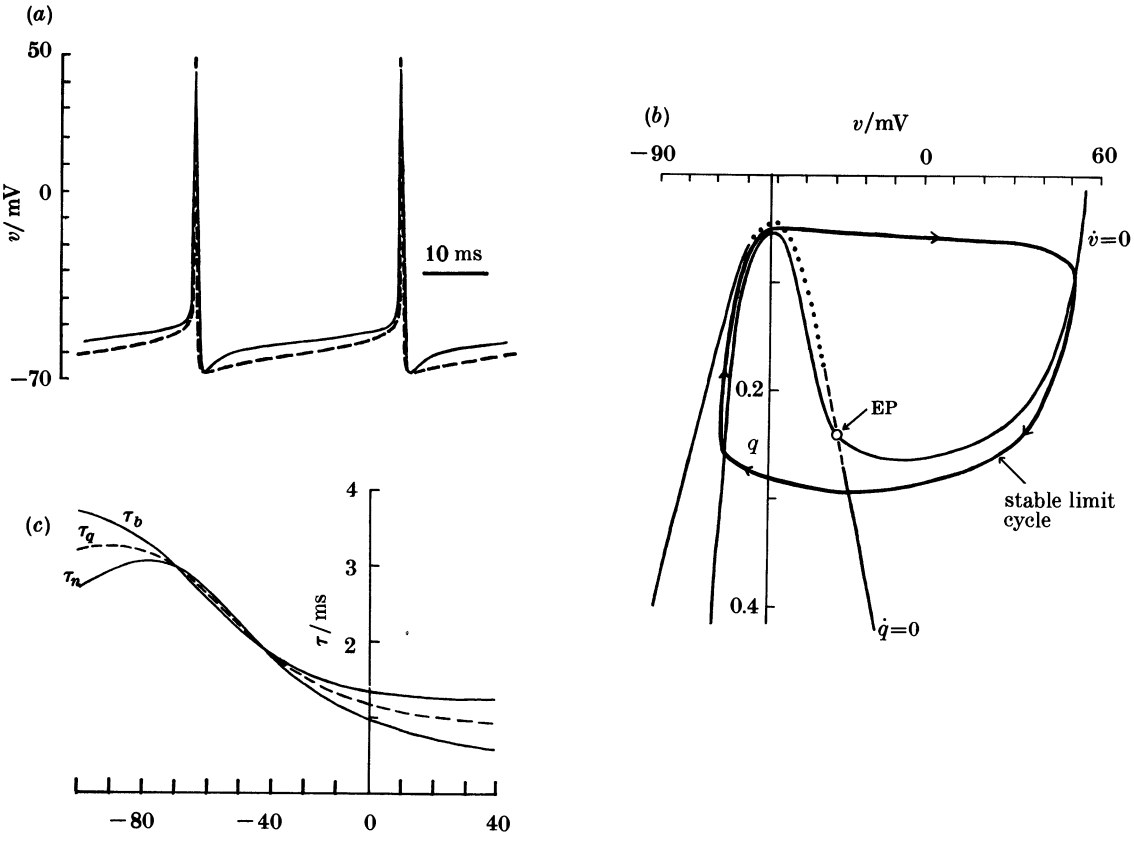

FIGURE 1. Repetitive-firing model with parameter values given in Appendix A. (*a*) Comparison of numerical solutions for six-dimensional system (equation (5)) with $I = 7$ μA cm^{-2} shown as solid line, and two-dimensional approximation (equation (9)) with $I = 7.6$ μA cm^{-2} shown as broken line (*b*) Narrow channel between $\dot{q} = 0$ and $\dot{v} = 0$ nullclines in the subthreshold region of the v, q phase–plane of the two-dimensional system. The EPs occur at the intersection of the v-nullcline, whose position varies with I, and the q-nullcline, which is fixed. Points on the q nullcline where the EP will be a saddle are shown as a dotted line, an unstable node or spiral as a broken line, and a stable EP as a solid line. In the example shown the single unstable EP is surrounded by a stable limit cycle corresponding to the firing of the two-dimensional system in (*a*). (*c*) Plot of $\tau_n(v)$ and $\tau_b(v)$ for the repetitive-firing model and their average $\tau_q(v)$ (broken line).

not introduced the q variable but made the same approximations for m, h, a and b, then we would have arrived at the equations

$$\dot{v} = C^{-1}[-g_{\mathrm{Na}}\, m_\infty^3(v)\,(-3n^4+0.85)\,(v-v_{\mathrm{Na}}) - g_L(v-v_L) - g_{\mathrm{K}}\, n^4(v-v_{\mathrm{K}}) - g_A\, 0.21 b_\infty(v-v_{\mathrm{K}}) + I],$$

$$\dot{n} = \tau_n^{-1}(v)\,[n_\infty(v) - n].$$

The nullclines for these equations are not in close proximity.

As we show later, the advantage of choosing q as a variable instead of n is that it makes it easier to include additional ionic currents whose effect is to distort the nullclines in the narrow channel region.

Addition of subthreshold currents

In our earlier model of neuronal bursting (Hindmarsh & Rose 1984) we modified our repetitive-firing model (Hindmarsh & Rose 1982) by making a small deformation of the y nullcline in the narrow channel region to create two additional equilibrium points. We suggested that this deformation could correspond to the presence of a subthreshold inward current. To terminate each burst we also added a slow adaptation current, giving a system of three differential equations. We now make similar additions to the present model, to give the equation

$$\left.\begin{aligned}\dot{v} &= C^{-1}[-g_{\mathrm{Na}}\, m_\infty^3(v)\{-3[q-Ab_\infty(v)]+0.85\}(v-v_{\mathrm{Na}})-g_L(v-v_L)\\ &\quad -g_{\mathrm{K}}\, q(v-v_{\mathrm{K}})-g_{s_a}\, s_{a_\infty}(v)(v-v_{xa})-g_{\mathrm{out}}\, z(v-v_{\mathrm{K}})+I],\\ \dot{q} &= \tau_q^{-1}(v)[q_\infty(v)-q],\\ \dot{z} &= \tau_z^{-1}[z_\infty(v)-z].\end{aligned}\right\} \tag{10}$$

In these equations we have introduced a subthreshold inward current whose equilibrium potential is v_{xa}. In the model of burst generation given below, I_{s_a} is a Na^+ current and $v_{xa}=v_{\mathrm{Na}}$, whereas in the model of a thalamic neuron given below I_{s_a} is a Ca^{2+} current and $v_{xa}=v_{\mathrm{Ca}}$. The I_{s_a} current is assumed to activate so rapidly that for a given voltage it is given by its steady-state value $g_{s_a}\, s_{a_\infty}(v)(v-v_{xa})$. Here g_{s_a} is the conductivity, and the steady-state value of the activation variable s_{a_∞} is given by

$$s_{a_\infty}(v)=\{1+\exp[-\gamma_{s_a}(v-\theta_{s_a})]\}^{-1}.$$

The parameters γ_{s_a} and θ_{s_a} determine the maximum slope and location on the v-axis of this S-shaped function of v. To terminate bursts we have also introduced a slow outward current I_z given by $I_z=g_{\mathrm{out}}\, z(v-v_{\mathrm{K}})$. For simplicity the activation variable z is also assumed to have a voltage-dependent steady-state value $z_\infty(v)$ given by $z_\infty(v)=\{1+\exp[-\gamma_z(v-\theta_z)]\}^{-1}$. We now have to choose values for the parameters introduced above. Choosing values for θ_{s_a} and γ_{s_a} amounts to specifying the voltage range in which the subthreshold inward current is activated. We refer to this choice as 'locating the current'. Similarly we have to locate the slow outward current.

To investigate the effect of the addition of the subthreshold inward current, we now remove the $\dot{z}$ equation and replace $I-I_z$ by J (constant) in equation (10), and plot the nullclines of the remaining two-dimensional system:

$$\left.\begin{aligned}\dot{v} &= C^{-1}[-g_{\mathrm{Na}}\, m_\infty^3(v)\{-3[q-Ab_\infty(v)]+0.85\}(v-v_{\mathrm{Na}})-g_L(v-v_L)\\ &\quad -g_{\mathrm{K}}\, q(v-v_{\mathrm{K}})-g_{s_a}\, s_{a_\infty}(v)(v-v_{xa})+J],\\ \dot{q} &= \tau_q^{-1}(v)[q_\infty(v)-q].\end{aligned}\right\} \tag{11}$$

If the subthreshold current, I_{s_a}, is located at $\theta_{s_a}=-58$ mV, then for the parameter values given in Appendix B two additional EPs are created in the narrow channel region. The resulting nullcline diagram (figure 2*a*) is similar to that of our earlier model of bursting (Hindmarsh & Rose 1984).

To locate the slow outward current, I_z, we shall show later that it is necessary to

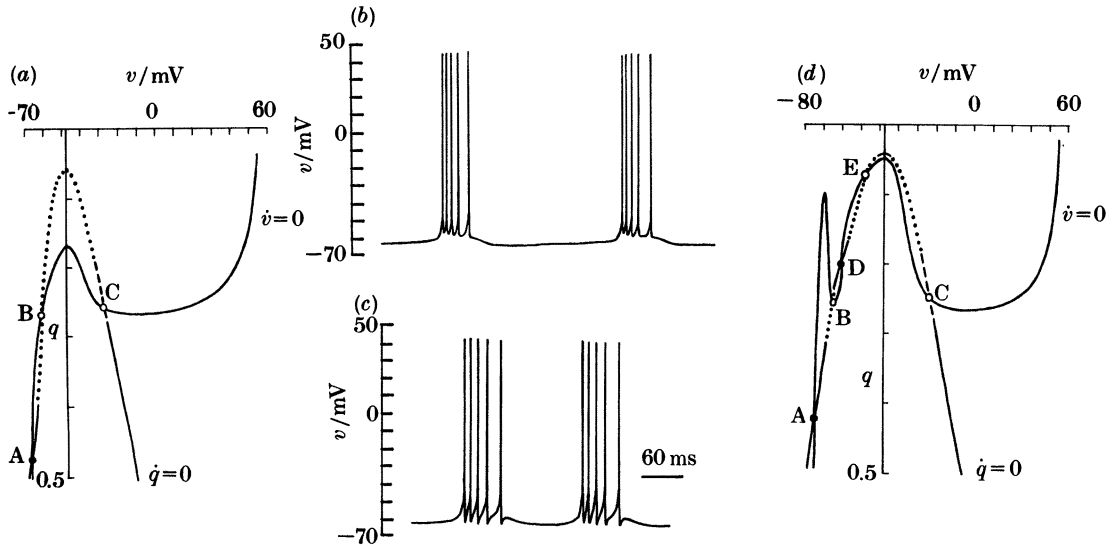

FIGURE 2. Nullcline diagrams and numerical solutions of equations (10)–(12). (*a*) Nullcline diagram of equation (11) showing three EPs. $J = 25\ \mu A\ cm^{-2}$, and other parameter values are those of the burst model give in Appendix B. The EPs A, B and C are a stable node or spiral, saddle EP, and unstable node or spiral respectively. (*b*) Numerical solution of three-dimensional system (equation (10)) with $I = 30\ \mu A\ cm^{-2}$ and $\tau_z = 66.7$ ms. (*c*) Numerical solution of seven-dimensional system (equation (12)) with $I = 30\ \mu A\ cm^{-2}$, $\tau_z = 166.7$ ms (*d*) Nullcline diagram of equation (11) showing five EPs. $J = -15\ \mu A\ cm^{-2}$, and other parameter values are those of the standard z-model give in Appendix C. The additional EPs, D and E, are a stable node or spiral and a saddle EP respectively.

consider the v, z projection of the full three-dimensional system. Rather than give an exhaustive account of the three-dimensional system for both bursting and thalamic models, we shall restrict discussion to the thalamic model. A similar analysis to that given in the next section shows that periodic bursting may be obtained by using equation (10) with the parameter values give in Appendix B, as shown in figure 2*b*.

Having located these two additional currents, I_z and I_{s_a}, we then added them and the equation for $\dot{z}$ to the repetitive firing model (equation (5)) to obtain the following seven-dimensional system:

$$\left.\begin{aligned}
\dot{v} &= C^{-1}[-g_{\mathrm{Na}}\, m^3 h(v-v_{\mathrm{Na}}) - g_L(v-v_L) - g_{\mathrm{K}}\, n^4(v-v_{\mathrm{K}}) - g_A\, a^3 b(v-v_{\mathrm{K}}) \\
&\quad - g_{s_a}\, s_{a_\infty}(v)\,(v-v_{xa}) - g_{\mathrm{out}}\, z(v-v_{\mathrm{K}}) + I], \\
\dot{m} &= \tau_m^{-1}(v)\,[m_\infty(v) - m], \\
\dot{n} &= \tau_n^{-1}(v)[n_\infty(v) - n], \\
\dot{h} &= \tau_h^{-1}(v)\,[h_\infty(v) - h], \\
\dot{a} &= \tau_a^{-1}(v)\,[a_\infty(v) - a], \\
\dot{b} &= \tau_b^{-1}(v)\,[b_\infty(v) - b], \\
\dot{z} &= \tau_z^{-1}[z_\infty(v) - z].
\end{aligned}\right\} \qquad (12)$$

With the same parameter values as given for the three-dimensional system (figure 2*b*) but with $\tau_z = 166.7$ instead of 66.7 ms (see legend of figure 2), equation (12) also has a periodic bursting solution as shown in figure 2*c*.

The similarity between the three-dimensional and seven-dimensional models of bursting was sufficiently close to encourage us to look for a five EP model similar to our earlier thalamic model (Rose & Hindmarsh 1985). The reason for wanting five EPs is to get a low-voltage stable EP, a mid-voltage stable EP and a suprathreshold unstable EP around which firing takes place, separated by two saddle EPs. An unexpected finding is that if the channel is lengthened by shifting α_i and β_i $(i = n, m, h)$ by 15 mV to the right along the voltage axis ($\sigma = 15$ mV, see Appendix A), and if θ_{s_a} is also moved further to the left ($\theta_{s_a} = -66$ mV) on the voltage axis, then we obtain a nullcline diagram with 5 EPs (figure 2*d*). This configuration is similar to that of our earlier model of a thalamic neuron (Rose & Hindmarsh 1985), in that it has two subthreshold stable EPs. We had previously thought that the occurrence of five EPs would require the presence of at least two subthreshold inward currents and had not expected that this could happen with just a single inward current. The parameter values for figure 2*d*, which are given in Appendix C, are used later as the basis of the thalamic model to be discussed in the next section.

The model of bursting that we have just discussed differs from most earlier models of bursting (Plant 1981; Kopell & Ermentrout 1986; Rinzel 1985, 1987; Rinzel & Lee 1986) in that these models lack the A-current. This suggests that it may be possible to construct a five EP model without the A-current. The A-current allowed us to construct a parabolic nullcline and consequently the narrow channel property. Without the A-current we would have a sigmoidal q nullcline ($q_\infty(v) = n^4_\infty(v)$) and the desired five EPs could still be obtained with a sufficiently large distortion of the v nullcline. However, the necessary changes can be made more simply if the A-current is present.

Three-dimensional thalamic model

Jahnsen & Llinás (1984*a*, *b*) showed that thalamic neurons have three different responses to a current step of fixed amplitude when it is applied to the cell hyperpolarized by a steady background current, at rest and depolarized by a steady background current. We shall call these the burst, resting and tonic responses to an applied current step at different values of initial membrane potential. To produce these responses by using the nullcline configuration shown in figure 2*d*, we first have to consider how to choose the parameter values for the slow outward current. To choose these values five conditions have to be satisfied.

(1) $I_z = 15\ \mu\text{A cm}^{-2}$ at $v = -61.5$ mV. In the nullcline diagram of figure 2*d* the stability of the EPs alternates in the sequence SUSUU, moving from left to right. Because the middle EP (at $v = -61.5$ mV) is to be the stable resting point (with $I = 0\ \mu\text{A cm}^{-2}$ in equation (10)), we must ensure that $I_z = 15\ \mu\text{A cm}^{-2}$ at $v = -61.5$ mV as the nullclines of the two-dimensional system (figure 2*d*) were drawn with $J = -15\ \mu\text{A cm}^{-2}$, and J is replaced by $I - I_z$ in the three-dimensional system.

2. $z_\infty(v) \approx 1$ for $v > -61.5$ mV. This is to ensure that z does not change for voltages above -61.5 mV, so that if a step in current is applied when the system is at rest (at $v = -61.5$ mV), the voltage will jump to a new value and remain there, as in the recordings of Jahnsen & Llinás (1984*a*, *b*). If condition (2) is not satisfied, the membrane potential will sag when the step is applied because z will change. This is not usually observed experimentally in thalamic neurons.

(3) $1 < g_{\text{out}} < 2$ mS cm^{-2}. If g_{out} takes higher values the slow outward current terminates the burst too quickly. If g_{out} takes smaller values the frequency of tonic firing will be too high.

(4) $-70 < \theta_z < -65$ mV, so that $z_\infty(v) \approx 0$ for v near -72 mV, and $z_\infty(v) \approx 1$ for v near -61.5 mV. This activation change is essential to obtain the burst response.

(5) γ_z should be large enough to achieve the requirements of condition (4).

By using these five conditions we chose the following values: $\theta_z = -68$ mV, $\gamma_z = 0.65$ mV^{-1}, $g_{\text{out}} = 1.449$ mS cm^{-2}.

Now that we have established how to include the slow outward current, we can proceed with a more detailed analysis of equation (10).

In our earlier qualitative model of a thalamic neuron (Rose & Hindmarsh 1985) we also used a three-dimensional system of differential equations to describe the burst, rest and tonic responses of thalamic neurons. Although the three-dimensional model given by equation (10) can also give these three responses if the parameter values are properly chosen, there is a significant difference between the two models that is relevant to the way in which we describe how the models work. We therefore begin by comparing these two models.

(*a*) *Comparison with the earlier thalamic model*

In our earlier models of bursting (Hindmarsh & Rose 1984) and of a thalamic neuron (Rose & Hindmarsh 1985) we discussed equations of the general form given by equation (2).

In these equations z was slowly varying, so that we were able to discuss the firing patterns by setting $I - z = J$ (constant) and plotting the nullclines of the two-dimensional system $\dot{x} = F(x) - y + J$, $\dot{y} = G(x) - y$. The x-nullcline is given by

---

Description of plate 1

Figure 3. (*a*) Diagram of the three-dimensional phase space of equation (10) showing the nullsurfaces for v with $I = 8$ μA cm^{-2} (in blue), q (in red) and z (in green). The three nullsurfaces intersect at the EP labelled A′. Also shown is the phase path (in yellow) during the burst response. (*b*) This is the same diagram as in (*a*), as seen from above. The red–blue boundary, labelled $\dot{v} = \dot{q} = 0$, is the v,q-nullcurve. The z-nullsurface, which is vertical in (*a*), now appears as a curve (shown in green). Note that at the termination of the burst the phase path moves along the v,q-nullcurve towards the EP at A′.

Figure 4. (*a*) As figure 3*a* except that $I = -15$ μA cm^{-2}. With this value of I the v-nullsurface (shown in blue) is different when compared with figure 3*a*, but the q-nullsurface (shown in red) and the z-nullsurface (shown in green) are unchanged. For this value of I all three nullsurfaces intersect at the EP labelled A. At the end of the burst response the phase path (shown in yellow) returns from its position close to A′ in figure 3 to the EP at A. (*b*) This is the same diagram as in (*a*) seen from above. Note how the v,q-nullcurve has changed shape compared with figure 3*b*.

3

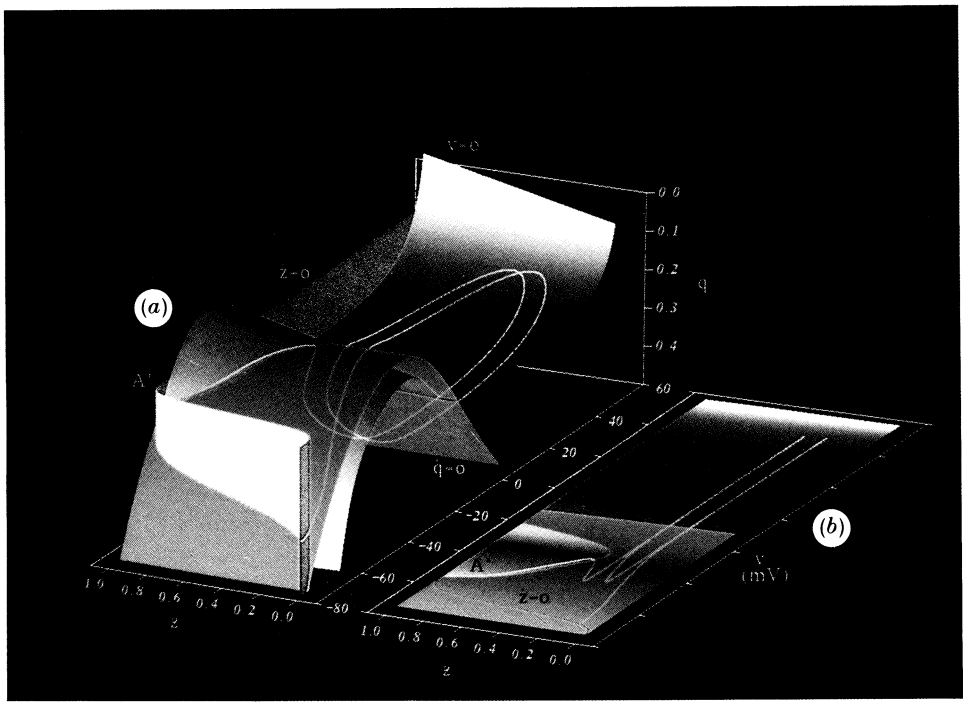

4

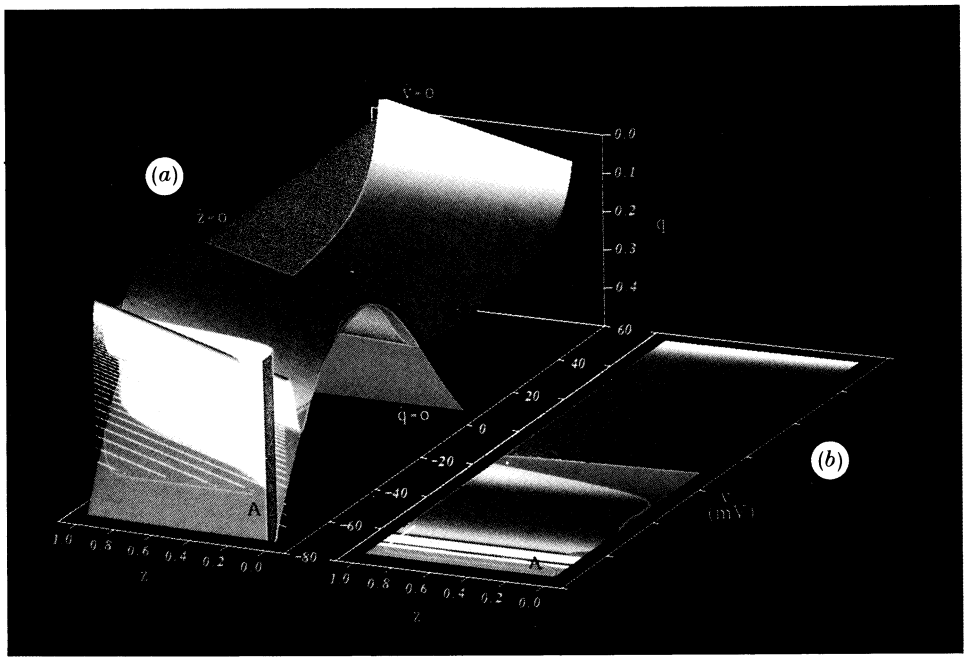

FIGURES 3 AND 4. For description see opposite.

$y = F(x) + J$, so the effect of changing z or I is simply to displace this nullcline vertically relative to the fixed y-nullcline. This displacement created and destroyed EPs and allowed us to explain the firing patterns.

With the new system of equations, (equation (10)), v and q have similar rôles to x and y. If we take the first two equations of (10) we are left with a two-dimensional system of the form

$$\left.\begin{aligned} v &= f_1(v) + f_2(v)\, q + f_3(v)\, z + C^{-1} I \\ q &= \tau_q^{-1}(v)\, [q_\infty(v) - q], \end{aligned}\right\} \tag{13}$$

whose v-nullcline is of the form $q = f_4(v) + f_5(v)\, z + f_6(v)\, I$, where $f_i(v)$ $(i = 1\text{–}6)$ is a function of v, and the effect of changing z or I is no longer simply to move this nullcline vertically. For this reason we have found that the clearest way to understand how the model behaves, and to locate the additional currents, is to consider the full three-dimensional model.

(*b*) *The nullsurfaces of the three-dimensional model*

For a three-dimensional system such as (10), the set of points in the phase space where $\dot{v} = 0$ is a two-dimensional surface, the v-nullsurface. Similarly we have a q-nullsurface and a z-nullsurface. In figures 3*a* and 4*a*, plate 1, the v-nullsurface is shown in blue, the q-nullsurface in red and the x-nullsurface in green. Note that in the front section of figure 4*a* (where $z = 0$) the v- and q-nullsurfaces have exactly the same configuration as in figure 2*d* because the parameter values are identical.

Any point common to all three nullsurfaces is an EP. If we vary I, the q- and z-nullsurfaces will not change but the v-nullsurface will. Thus the EPs may change position as I varies but they must remain on the curve where the q-nullsurface and the z-nullsurface intersect. For example, for the burst response the system is initially at the EP labelled A in figure 4*a*. With an increase in I, the v-nullsurface changes and the EP changes position to the point labelled A′ in figure 3*a*.

(*c*) *Temporary equilibrium points*

Let us now consider the consequences of the fact that z is slowly varying. We can do this approximately by setting $z = z_0$ (constant) so that the motion of the phase point is confined to the plane $z = z_0$. The v and q nullclines of this two-dimensional system are simply the intersection of the v- and q-nullsurfaces of the three-dimensional model with the plane $z = z_0$. The intersection of these v- and q-nullclines is an equilibrium point of the two-dimensional system. To distinguish such an equilibrium point from an equilibrium point (EP) of the three-dimensional system we will refer to it as a temporary equilibrium point (TEP). A TEP must lie on the q-nullsurface, which is fixed, its position in that surface being determined by the choice of z_0 and I. Changing I changes the v-nullsurface and hence changes the points of intersection of the v- and q-nullsurfaces and the $z = z_0$ plane.

In plate 1, the TEPs of the two-dimensional system in the plane $z = z_0$ are the points in that plane at which the blue and red nullsurfaces intersect. In the v, z projection (figures 3*b*, plate 1, and 4*b*, plate 1) these points of intersection occur along the line where the colour changes between blue and red. Figure 5*b*, *c* is the

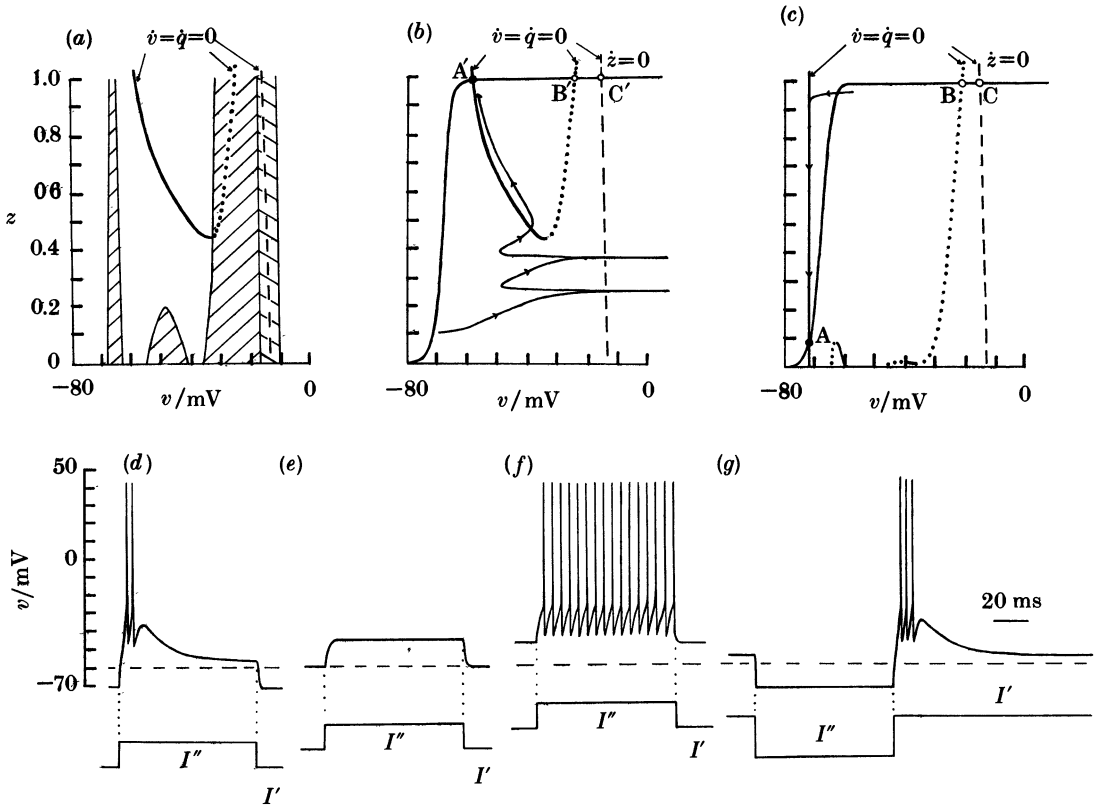

FIGURE 5. Standard z-model with parameter values given in Appendix C. (a) Stability diagram with v, q-nullcurve for $I = 8$ μA cm^{-2} superimposed. (b) Movement of phase point projected onto v, z plane during application of a current step that gives the burst response shown in (d). v, q-nullcurve is shown for $I = -15$ μA cm^{-2} (before and after the current step is applied) in (c), and for $I = 8$ μA cm^{-2} (during the current step) in (b). For further explanation see text. (d–f) Responses to a current step, I'', of 23 μA cm^{-2} amplitude and 80 ms duration for different values of I'. In (d), $I' = -15$ μA cm^{-2}, $v(0) = -71.5$ mV; (e) $I' = 0$ μA cm^{-2}, $v(0) = -61.5$ mV; (f) $I' = 18$ μA cm^{-2}, $v(0) = -50$ mV. (g) Post-inhibitory rebound in response to a current step, I'', of -40 μA cm^{-2} amplitude and 80 ms duration with $I' = 10$ μA cm^{-2} and $v(0) = -55$ mV.

same as figures 3b and 4b but the line where the v- and q-nullsurfaces intersect has been labelled $\dot{v} = \dot{q} = 0$. Also shown in figures 3b and 4b and figure 5b, c is the projection of the vertical S-shaped z-nullsurface (where $\dot{z} = 0$). The leftmost point where the $\dot{z} = 0$ curve intersects the $\dot{v} = \dot{q} = 0$ curve in figure 4 corresponds to the EP labelled A in figure 5c. In this and subsequent diagrams, stable EPs are denoted by a filled circle and unstable EPs are denoted by an open circle.

(d) *Stability regions*

If the three-dimensional system is in a state that coincides with a TEP of a two-dimensional system with constant z then in that state $\dot{v} = 0$ and $\dot{q} = 0$ but $\dot{z} \neq 0$ in general. The evolution of a state of the three-dimensional system that is near a TEP of a two-dimensional system in the plane $z = z_0$ can be obtained from the

stability type of that TEP. As the coordinates (v_0, q_0, z_0) of a TEP have $q_0 = q_\infty(v_0)$ we can refer to a TEP by its v and z coordinates alone. The stability of a TEP is obtained in the usual way from (11) and depends on its v and z coordinates but not on I. In this way we obtain figure 5*a*, which we call a stability diagram. This shows the stability type of any TEP in the q-nullsurface according to the following convention, which we use in this and the following paper (Rose & Hindmarsh 1989*a*): regions where the TEPs are of saddle type are shown hatched bottom left to top right, regions where they are of unstable node or spiral type are shown hatched top left to bottom right, and all stable regions are unshaded.

Note that this stability diagram is more complicated than the corresponding stability diagram would be for our earlier model (Rose & Hindmarsh 1985). In the earlier model the stability of a TEP does not depend on z, with the consequence that the stability regions are bands of constant width parallel to the z-axis.

When all the parameters (except I) have been chosen, the stability diagram of the system is determined, and to a certain extent specifies the system.

The stability diagram is used as follows. For a given value of I we superimpose on the stability diagram the projection of the curve $\dot{v} = \dot{q} = 0$. We call this curve the v, q-nullcurve. The configuraton of this curve will of course vary with I. Then for any value of z_0 the TEPs occur where the line $z = z_0$ intersects the v, q-nullcurve. Finally the stability of these TEPs is obtained from the stability diagram. The v, q-nullcurve can then be divided into sections where TEPs on the curve are stable (solid curve), sections where they are unstable saddle points (dotted curve), and sections where they are unstable nodes or spirals (dashed curve). Again we use this convention in the following paper (Rose & Hindmarsh 1989*a*).

(*e*) *Responses to current steps*

We shall describe a current step by giving the value of the constant current, I', to which is added the value of the step current, I''. Thus during the application of the current step the total current, I, is given by $I = I' + I''$. We first explain the movement of the phase point during the burst response. Figures 3 and 4, or equivalently figure 5*b*, *c*, will be used to explain the burst response shown in figure 5*d*.

Before the current step is applied, the system is at EP A, which is stable (figure 4*a*, *b*). On application of the current step the v-nullsurface changes shape (figure 3*a*) and the EP moves to the point labelled A′, which is also stable. In moving from A to A′ the phase point undergoes slow movements when it is in the subthreshold region and close to the v- and q-nullsurfaces, and rapid movements corresponding to action potentials when above threshold. To distinguish between these two types of movement we shall refer to the rapid movements as 'action cycles'. The slower movement, which would still take place if g_{Na} were set equal to zero, corresponds to what Jahnsen & Llinás (1984*a*, *b*) referred to as the low threshold spike (LTS). The v, z projections (figures 3*b* and 4*b*) can be used to understand these movements because for most of the time the movement of the phase point is confined to the subthreshold region where the linear approximation can be applied to determine the stability type of the TEPs.

The burst response begins with two action cycles, there being a single unstable

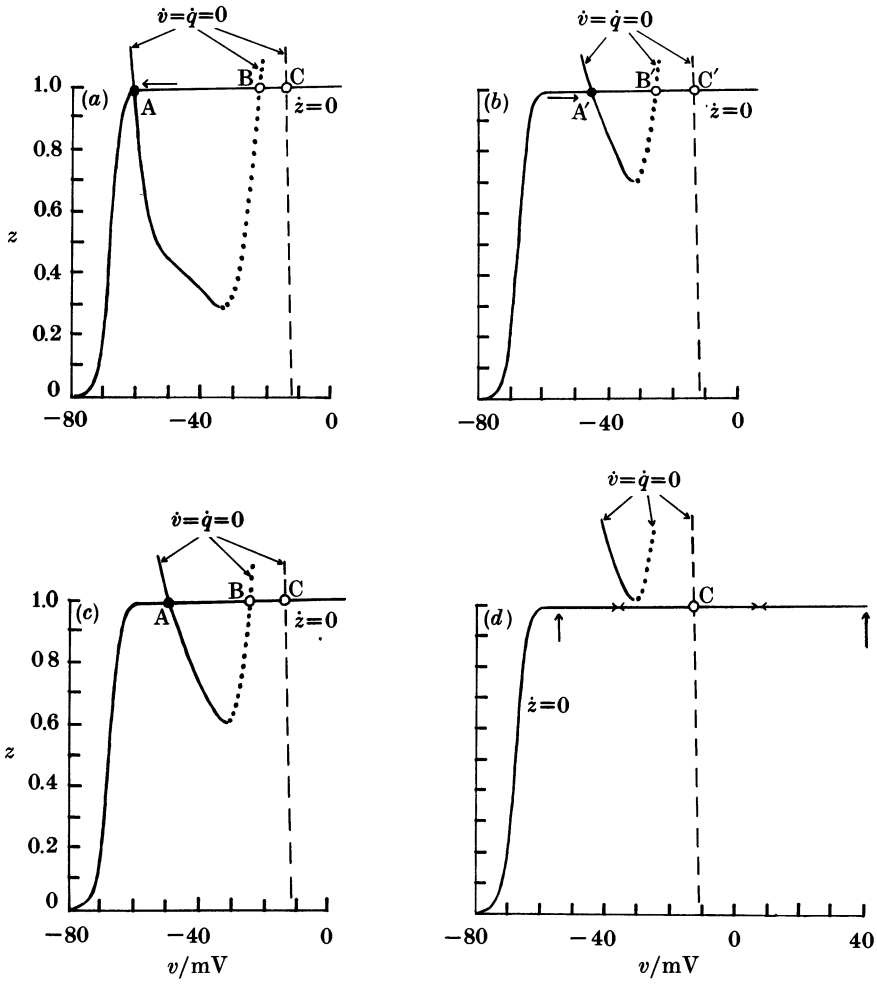

FIGURE 6. Explanation of resting and tonic responses of figure 5*e*, *f*. (*a*) System is at the stable EP at A. (*b*) During application of current step, phase point moves to a new EP at A′ (rest response). At end of current step phase point moves to a new EP at A (arrow in (*a*)). (*c*) At a more depolarized level the system is at the stable EP at A. (*d*) During application of current step there is a single unstable EP at C′ and tonic firing takes place with the phase point moving backwards and forwards between the vertical arrows. Numerical values given in text.

TEP above spike threshold and no TEPs in the subthreshold region. When the phase point moves to the right in the subthreshold region for the third time, z has increased to $z \approx 0.5$, at which point the phase point turns to the left, moving away from the saddle TEPs and towards the stable TEPs to approach the single stable EP, A′. This movement is seen most clearly in the v, z projection (figure 3*b*).

Just before the current step is terminated the phase point is close to EP A′. When the current step goes off, we return to the nullsurface diagrams of figure 4*a*, *b* to understand the movement from A′ to A. Initially the phase point moves rapidly towards the intersection of the v- and q-nullsurfaces to the left of the z-nullsurface.

It then follows the line of stable TEPs at this intersection as z decreases until the EP at A is reached.

The resting and tonic responses shown in figure 5*e*, *f* can be understood by constructing similar diagrams (figure 6). At rest ($I' = I'' = 0$ μA cm^{-2}) the system is at the stable EP A ($v = -61.5$ mV, figure 6*a*). Application of a current step $I'' = 23$ μA cm^{-2} displaces the v, q-nullcurve upwards to give a new stable EP at A′ ($v = -54$ mV, figure 6*b*). The movement of the phase point is from A to A′ along the z_∞ curve as shown by the arrow in figure 6*b*. On termination of the current step the phase point moves back to A, as shown by the arrow in figure 6*a*.

For the tonic response we start with $I' = 18$ μA cm^{-2} and with the system at the stable EP A ($v = -50$ mV, figure 6*c*). Application of a current step $I'' = 23$ μA cm^{-2}, displaces the v, q-nullcurve upwards so that it now intersects the z_∞ curve at a single unstable EP C′ (figure 6*d*). Firing now takes place with the phase point moving backwards and forwards between the arrows shown in figure 6*d*.

We note from figure 5*d*, *f* that the frequency of burst firing is very similar to the frequency of tonic firing. Experimentally Jahnsen & Llinás (1984*a*, *b*) found that for the same amplitude current step the frequency of tonic firing was much lower than that which occurs during bursting. They gave experimental evidence that this difference was caused by the activation of a Ca^{2+}-activated K^+ current, $I_{K(Ca)}$, during tonic firing. We have also found that the addition of a slow outward current to equation (10) can produce this frequency difference. The essential requirements are that the additional outward current activates in the voltage range where tonic firing take place, and that it has a slow time constant. Because of the slow time constant this current does not activate significantly during burst firing. Because the effect of adding this current is to provide a steady hyperpolarizing current in the tonic firing range, we can obtain similar results by reducing the amplitude of the current step I'' required to obtain the tonic response. At this stage we shall avoid the addition of a fourth differential equation, as we wish to retain the simplicity of the three-dimensional system.

The rebound response shown in figure 5*g* is essentially the burst response in reverse, except that we found that it was necessary to apply a steady depolarizing current ($I' = 10$ μA cm^{-2}) to obtain rebound firing. Thus the system starts off at −55 mV, and during the hyperpolarizing step the phase point moves as shown in figure 5*c* except that the voltage is driven to a more negative value. On release from the current step the movement of the phase point is similar to that shown in figure 5*a*, *b* and a rebound burst is generated.

Having established that we can obtain these different responses by using the three-dimensional model (equation (10)), the final step is to confirm that the complete seven-dimensional model (equation (12)) can give similar solutions.

Seven-dimensional thalamic model

Beginning with the same parameter values as those in the three-dimensional thalamic model shown in figures 3–6, we now have to choose values for the m, a and h variables to return to the complete seven-dimensional model. There is considerable freedom in choosing these parameter values, and we have simply used

the values of the repetitive-firing model (Appendix A) with a few simple modifications given in the legend of figure 7. As shown in figure 7, numerical integration of equation (12) with these parameter values gives burst, rest, tonic and rebound responses provided that we choose new values for I' and I''. In this case we have not calculated the stability diagram and the nullcurves to explain the burst response because at this stage we were only interested in establishing that it was possible to return to the seven-dimensional system (see Discussion).

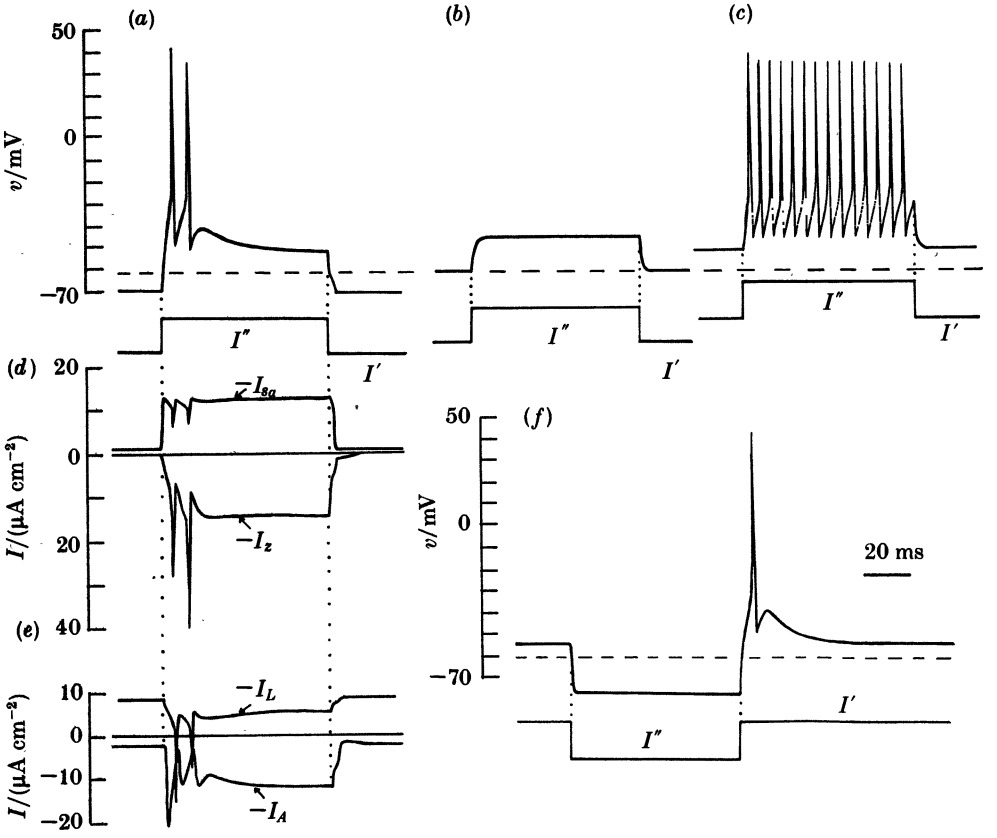

FIGURE 7. Seven-dimensional z-model (equation (12)) with parameter values the same as those of the standard three-dimensional z-model (Appendix C) and with $T_m = T_h = 0.066$, $T_a = 0.25$ and h_∞ as in the repetitive-firing model (Appendix (A)) with $\sigma = 15$ mV. (q–c) Responses to a current step, I'', of 30 μA cm^{-2} amplitude and 80 ms duration for different values of I'. In (a) $I' = -11.2$ μA cm^{-2}, $v(0) = -70$ mV; (b) $I' = 0$ μA cm^{-2}, $v(0) = -61.5$ mV; and (c) $I' = 20$ μA cm^{-2}, $v(0) = -52$ mV. (d–e) Timecourses of ionic currents during the burst response shown in (a). (f) Post-inhibitory rebound in response to a current step, I'', of -30 μA cm^{-2} amplitude and 80 ms duration with $I' = 10$ μA cm^{-2} and $v(0) = -55$ mV.

Below the burst response of figure 7 a we have also plotted the timecourses of the different ionic currents. These currents have been plotted so that the applied current step, I'', is plotted in the same direction as in previous examples. This is the opposite of the usual voltage-clamp convention in which inward currents are

plotted in the downward direction, but facilitates comparison with the previous results. Also only four of the six ionic currents in equation (12) have been plotted, the fast I_{Na} and $I_{K(v)}$ currents being omitted as they contribute little to the membrane potential changes in the subthreshold region.

As shown in figure 7*d* there is an initial rise in the inward I_{s_a} current when the current step is applied, this being counteracted by a rapid rise in the outward I_A current (figure 6*e*). Throughout the burst response all four subthreshold currents contribute to the membrane potential change. The falling phase of the LTS occurs as the result of a fine balance between the outward I_A and I_z currents and the inward I_{s_a} and leakage currents, with the outward currents gradually predominating.

The steady-state current–voltage relations for each of the six currents present in the model are shown in figure 8*a*. The total steady-state current is shown in figure 8*b*. The individual currents, apart from I_z and I_{s_a}, are similar to those shown in figure 8 of Connor *et al.* (1977). Note that the currents we have added can be compared with the sodium and potassium currents of the action potential in that the inward current activates faster than the outward current and in that they approximately balance in the steady state. This comparison may be extended by regarding the LTS as a slow action potential.

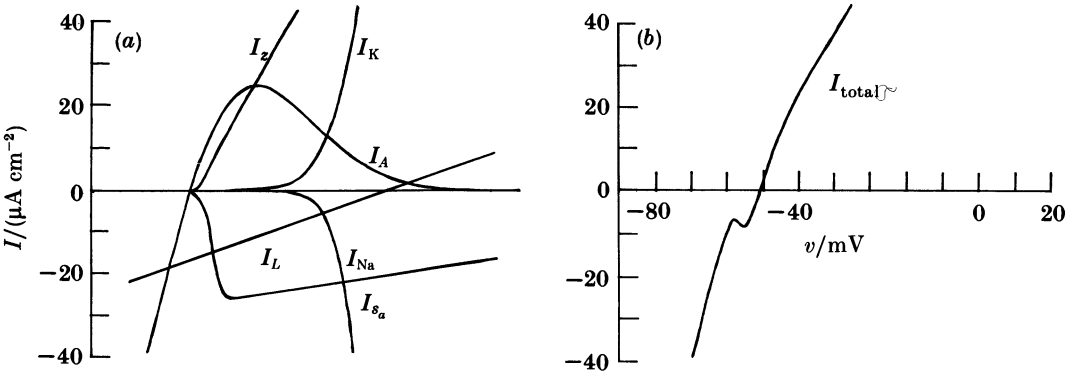

FIGURE 8. (*a*) Steady-state current–voltage relations of the individual ionic currents for the seven-dimensional z-model. (*b*) Total steady-state current–voltage relations. Parameter values as in figure 7.

These plots of the ionic current changes lead us to question the validity of our model of a thalamic neuron. One problem is that in our model the LTS is caused by the activation of a maintained I_{s_a} current that is opposed by a slowly rising outward I_z current during the falling phase. By contrast Jahnsen & Llinás (1984*a*, *b*) suggested that the falling phase of the LTS was caused by voltage-dependent inactivation of a current similar to I_{s_a}. In the following paper (Rose & Hindmarsh 1989*b*) we shall examine this alternative mechanism and develop a second model. We shall then have two models both capable of explaining a variety of firing patterns. Although present experimental evidence appears to favour the second model, we shall suggest that a complete description of a given cell type may well require a combination of both models.

Discussion

The aim of this paper was to replace our earlier qualitative models of repetitive firing (Hindmarsh & Rose 1982), bursting (Hindmarsh & Rose 1984), and of a thalamic neuron (Rose & Hindmarsh 1985) by models having variables of the Hodgkin–Huxley type. In the first of these earlier models we explained repetitive firing in terms of the close proximity of the nullclines in the phase-plane representation of a two-dimensional system, referring to this as the narrow channel. The burst and thalamic models resulted from making first one and then a second deformation of the nullclines of the narrow channel. Because the burst and thalamic models were dependent on the presence of the narrow channel, the first problem that we had to consider in this paper was how to obtain this feature by using equations of the Hodgkin–Huxley type. This first step involved the definition of the q variable.

The q variable

We showed above how it was possible to reduce the six-dimensional repetitive-firing model of Connor *et al.* (1977) to a two-dimensional system having the narrow channel feature. The six-dimensional model included a fast transient potassium (I_A) current. Therefore the first step made in this paper was to associate the narrow channel with the presence of an A-current in the cell. Consequently the results obtained in this and the following papers (Rose & Hindmarsh 1989*a*, *b*) only apply to neurons having an A-current. This may not be too severe a restriction, as this current has been found in many neurons since its original quantitative description in molluscan neurons by Connor & Stevens (1971). Rogawski (1985) has suggested that the A-current may have appeared early in evolution, possibly before the appearance of the fast Na^+ current. He also suggested that the squid axon may be a unique type of nerve membrane in its lack of the A-current. Whether this is correct or not, this current certainly appears to be present in thalamic neurons (Jahnsen &, Llinás 1984*a*, *b*).

The association between the presence of an A-current and the narrow channel feature was dependent on the definition of the q variable. Although the definition that we have given may appear straightforward, it was arrived at with some difficulty. This was because it was necessary for the definition to satisfy two further conditions besides being able to give the narrow channel. Firstly, the choice had to be made so that it was possible to proceed through the two succeeding stages of the bursting and thalamic models. For example, we initially used the definition $q = n^4 + (g_A/g_K)\, a_\infty^3\, b$. After a long investigation of the resulting differential equations we found that although it was possible to obtain a bursting model with this definition, the configuration of the nullclines was such that it was not possible to obtain a thalamic model.

The second condition on the choice of q was that it had to be possible at each stage in the development of the thalamic model to reverse the approximation and show that the solution of the corresponding complete system of equations was similar to that of the three-dimensional model. That this is so (see figures 1, 2 and 7) seems to result from the fact that there was very close agreement (see figure 1) between the reduced and complete systems for repetitive firing. In the following

paper we shall replace the three-dimensional model discussed here with an alternative three-dimensional model, and in the final paper (Rose & Hindmarsh 1989*b*) we shall give a complete analysis of the seven-dimensional system that corresponds to this new model. The type of analysis given for this alternative seven-dimensional model could also be applied to the seven-dimensional model discussed above. However, at this stage we simply wanted to satisfy ourselves that the return to the seven-dimensional model was possible at each of the three stages of the repetitive firing, bursting and the thalamic models. We shall not try to explain why this return has been successful until the above model has been modified.

Although the development of the thalamic model is dependent on the definition of the q variable, an equally important part of the paper is the analysis of the three-dimensional system. We now discuss some of the concepts involved in this analysis.

The three-dimensional model

The representation of firing in three dimensions would be expected to be much more complicated than a two-dimensional representation. This is clearly illustrated in figures 3*a* and 4*a*. In this case we needed two pictures of the nullsurfaces to visualize the evolution of the system when a current step was applied. If it was necessary to represent firing in this way for each experiment the description of the properties of thalamic neurons would be very complicated. Fortunately, as shown in figures 3*b* and 4*b*, the movements of the phase point can be represented more simply by using the projection to the v, z plane. This is possible for several reasons. Firstly, the action cycles are fast and are orientated vertically so that they appear as horizontal lines in the v, z projection. Secondly, the z-nullsurface (shown in green in figures 3 and 4) is a vertical sheet whose v, z projection is simply a curve. Thirdly because the z variable changes more slowly than v, we can consider the stability of the TEPs, which are the points of intersection of the v and q nullsurfaces in planes of constant z. This enables us to subdivide the $\dot{v} = \dot{q} = 0$ curve, which we have called the v, q-nullcurve, into sections where the TEPs are of different stability. The projection of the z-nullsurface, the v, q-nullcurve and the movement of the phase point, gives us a composite diagram in the v, z plane with which the firing pattern can be explained. We shall call this the state diagram for the system.

If we return to the bursting shown in figure 2*b* we find that the state diagram for this (v, q, z) system is similar to that used by Rinzel (1985, 1987) in his description of bursting in the pancreatic β-cell. Here Rinzel uses three variables (v, n, Ca), with internal calcium as the slow variable. His v, Ca plane is similar to our v, z plane, and his bifurcation diagram to our state diagram. One additional feature that Rinzel shows on the bifurcation diagram is the 'temporary' periodic solutions for the spiking phase of the burst. This feature could usefully be added to our representation of thalamic bursting.

The discovery that firing in a thalamic neuron can be represented by using the state diagram is really the most important feature of the model. To illustrate its importance, consider the burst model of Plant & Kim (1976). This model consisted of a complete system of six differential equations, which included the A-current, and was very similar to our complete model (equation (12)). Our complete equations are not therefore particularly original. However, our reduced three-

dimensional system (equation (10)) is original, and it is this system that allows us to develop the burst model into a thalamic model. Furthermore, the stability of the TEPS along the v, q nullcurve in this model is determined by the stability diagram. The stability diagram provides us with a visual representation of the assembly of the different ionic currents. In the following paper (Rose & Hindmarsh 1989*a*) we shall show how this stability diagram can be used together with the state diagram to produce different types of firing pattern that have been shown to exist in thalamic and other types of mammalian neuron.

This work was supported by the Wellcome Trust. We thank Chris Reynolds, Danny Ross and Dr Brian Rosser of the Mathematics and Computing Department, Polytechnic of Wales, for calculating and plotting figures 3 and 4. We also thank the referees for their valuable comments.

Appendix A. Repetitive firing

Connor *et al.* (1977) based their model of repetitive firing in the crab axon on the Hodgkin–Huxley equations for the squid axon (Hodgkin & Huxley 1952). First the Hodgkin–Huxley Na^+ and K^+ conductances were modified by shifting the voltage dependence of α_i, β_i $(i = n, m, h)$ to give a reasonable fit to voltage-clamp data from the crab axon. Secondly, they added an A-current.

In our model we take the equations of Connor *et al.* and add a parameter, σ, to allow us to apply a further, uniform, shift to the Na^+ and K^+ conductances. Thus our equations for the rate constants for m, h and n are

$$\alpha_m = \frac{-\frac{1}{10}(v+29.7-\sigma)}{\exp[-\frac{1}{10}(v+29.7-\sigma)]-1},$$

$$\beta_m = 4\exp[-\tfrac{1}{18}(v+54.7-\sigma)],$$

$$\alpha_h = 0.07\exp[-\tfrac{1}{20}(v+48-\sigma)],$$

$$\beta_h = \frac{1}{\exp[-\frac{1}{10}(v+18-\sigma)]+1},$$

$$\alpha_n = \frac{-\frac{1}{100}(v+45.7-\sigma)}{\exp[-\frac{1}{10}(v+45.7-\sigma)]-1},$$

$$\beta_n = 0.125\exp[-\tfrac{1}{80}(v+55.7-\sigma)].$$

For the repetitive-firing model, $\sigma = 0$ mV. The steady-state values and time constants are given by

$$m_\infty(v) = \alpha_m(v)/[\alpha_m(v)+\beta_m(v)], \quad \tau_m(v) = T_m/[\alpha_m(v)+\beta_m(v)],$$

$$h_\infty(v) = \alpha_h(V)/[\alpha_h(v)+\beta_h(v)], \quad \tau_h(v) = T_h/[\alpha_h(v)+\beta_h(v)],$$

$$n_\infty(v) = \alpha_n(V)/[\alpha_n(v)+\beta_n(v)], \quad \tau_n(v) = T_n/[\alpha_n(v)+\beta_n(v)],$$

whereas in the Connor *et al.* model all time constants in the Hodgkin–Huxley equations were scaled to 18 °C by setting $T_m = 0.26$, $T_h = 0.26$ and $T_n = 0.52$. In

the thalamic model given in Appendix C we have reduced these values to a quarter of their original values. The effect of this reduction was to speed up the recovery to obtain a better fit to the action potential undershoot.

The equations describing the A-current are

$$a_\infty(v) = \left[\frac{0.0761\exp[(v+94.22)/31.84]}{1+\exp[(v+1.17)/28.93]}\right]^{\frac{1}{3}},$$

$$\tau_a(v) = T_a\left[0.3632+\frac{1.158}{1+\exp[(v+55.96)/20.12)]}\right],$$

$$b_\infty(v) = \left[\frac{1}{\{1+\exp[\gamma_b(V+53.3)]\}}\right]^{\frac{1}{4}},$$

$$\tau_b(v) = T_b\left\{1.24+\frac{2.678}{1+\exp[(v+50)/16.027]}\right\},$$

where $T_a = T_b = 1$ and $\gamma_b = 0.069\ \mathrm{mV}^{-1}$ in the repetitive-firing model.

In the Connor *et al.* model the following equilibrium potentials and conductance values were used: $v_{\mathrm{Na}} = +55$ mV, $v_{\mathrm{K}} = -72$ mV, $v_A = -75$ mV, $v_L = -17$ mV, $g_{\mathrm{Na}} = 120\ \mathrm{mS\ cm^{-2}}$, $g_{\mathrm{K}} = 20\ \mathrm{mS\ cm^{-2}}$, $g_L = 0.3\ \mathrm{mS\ cm^{-2}}$, $g_A = 47.7\ \mathrm{mS\ cm^{-2}}$, and the membrane capacitance, C, was given the value of $1\ \mu\mathrm{F\ cm^{-2}}$. These are also the values used in our repetitive-firing model except that we have put $v_A = v_{\mathrm{K}} = -72$ mV.

Appendix B. Burst model

The parameter values for the three-dimensional burst model shown in figure 2 are the same as for the repetitive-firing model except that $\sigma = 0$ mV, $g_{\mathrm{K}} = 15\ \mathrm{mS\ cm^{-2}}$, $g_A = 90\ \mathrm{mS\ cm^{-2}}$ and $\gamma_b = 0.1\ \mathrm{mV^{-1}}$. The subthreshold current I_{s_a} is assumed to be a sodium current ($v_{\mathrm{xa}} = v_{\mathrm{Na}} = 55$ mV) with the following parameter values: $g_{s_a} = 0.2\ \mathrm{mS\ cm^{-2}}$, $\theta_{s_a} = -58$ mV and $\gamma_{s_a} = 0.3\ \mathrm{mV^{-1}}$. For the slow outward current, I_z, the following parameter values were used: $g_{\mathrm{out}} = 20\ \mathrm{mS\ cm^{-2}}$, $\theta_z = -40$ mV, $\gamma_z = 0.7\ \mathrm{mV^{-1}}$ and $\tau_z = 66.7$ ms.

Appendix C. Thalamic model

As z is our name for the conductance variable of the slow outward current, I_z, in equation (10), we refer to the thalamic model of this paper as the z-model to distinguish it from the h_a-model discussed in the following paper (Rose & Hindmarsh 1989*a*). The parameter values for the standard three-dimensional z-model are the same as for the repetitive-firing model except that $\sigma = 15$ mV, $g_{\mathrm{K}} = 10\ \mathrm{mS\ cm^{-2}}$, $g_A = 90\ \mathrm{mS\ cm^{-2}}$ and $\gamma_b = 0.1\ \mathrm{mV^{-1}}$. The subthreshold current I_{s_a} is assumed to be a Ca^{2+} current ($v_{\mathrm{xa}} = v_{\mathrm{Ca}} = 130$ mV) with the following parameter values: $g_{s_a} = 0.135\ \mathrm{mS\ cm^{-2}}$, $\theta_{s_a} = -66$ mV and $\gamma_{s_a} = 0.8\ \mathrm{mV^{-1}}$. For the slow outward current, I_z, the following parameter values were used: $g_{\mathrm{out}} = 1.449\ \mathrm{mS\ cm^{-2}}$, $\theta_z = -68$ mV, $\gamma_2 = 0.8\ \mathrm{mV^{-1}}$ and $\tau_z = 25$ ms. To reduce the undershoot of the fast action potentials we found that it was necessary to decrease the values of T_n and T_b to $T_n = 0.066$ and $T_b = 0.25$.

References

Connor, J. A. & Stevens, C. F. 1971 Prediction of repetitive firing behaviour from voltage-clamp data on an isolated neurone soma. *J. Physiol., Lond.* **213**, 31–53.

Connor, J. A., Walter, D. & McKown, R. 1977 Neural repetitive firing: modifications of the Hodgkin–Huxley axon suggested by experimental results from crustacean axons. *Biophys. J.* **18**, 81–102

Fitzhugh, R. 1961 Impulses and physiological states in theoretical models of nerve membrane. *Biophys. J.* **1**, 445–466.

Hagiwara, S., Kusano, K. & Saito, N. 1961 Membrane changes in *Onchidium* nerve cell in potassium-rich media. *J. Physiol., Lond.* **155**, 470–489.

Hindmarsh, J. L. & Rose, R. M. 1982 A model of the nerve impulse using two first order differential equations. *Nature, Lond.* **296**, 162–164.

Hindmarsh, J. L. & Rose, R. M. 1984 A model of neuronal bursting using three coupled first order differential equations. *Proc. R. Soc. Lond.* B **221**, 87–102.

Hodgkin, A. L. & Huxley, A. F. 1952 A quantitative description of membrane current and its application to conduction and excitation in nerve. *J. Physiol., Lond.* **117**, 500–544.

Jahnsen, H. & Llinás, R. 1984*a* Electropysiological properties of guinea-pig thalamic neurons: an *in vitro* study. *J. Physiol., Lond.* **349**, 205–226.

Jahnsen, H. & Llinás, R. 1984*b* Ionic basis for the electroresponsiveness and oscillatory properties of guinea-pig thalamic neurones *in vitro*. *J. Physiol, Lond.* **349**, 227–247.

Krinskii, V. I. & Kokoz, Y. M. 1973 Analysis of equations of excitable membranes – I. Reduction of the Hodgkin–Huxley equations to a second order system. *Biofizika* **18**, 533–539.

Kopell, N. & Ermentrout, G. B. 1986 Subcellular oscillations and bursting. *Math. Biosci.* **78**, 265–291.

Kokoz, Yu. M. & Krinskii, V. I. 1973 Analysis of equations of excitable membranes – II. Method of analysing the electrophysiological characteristics of the Hodgkin–Huxley membrane from the graphs of the zero-isoclines of a second order system. *Biofizika* **18**, 937–944.

Neher, E. 1971 Two fast transient current components during voltage clamp on snail neurons. *J. gen. Physiol.* **58**, 36–53.

Plant, R. E. 1976 The geometry of the Hodgkin–Huxley model. In *Computer programs in biomedicine*, vol. 6, pp. 85–91. Amsterdam: North Holland.

Plant, R. E. 1981 Bifurcation and resonance in a model for bursting nerve cells. *J. math. Biol.* **11**, 15–32.

Plant, R. E. & Kim, M. 1976 Mathematical description of a bursting pacemaker neuron by a modification of the Hodgkin–Huxley equations. *Biophys. J.* **16**, 227–244.

Rinzel, J. 1978 Integration and propagation of neuroelectric signals. In *Studies in mathematical biology I* (ed. S. A. Levin), pp. 1–66. Mathematical Association of America.

Rinzel, J. 1985 Bursting oscillations in an excitable membrane model. In *Ordinary and partial differential equations* (*Lecture notes in mathematics*, vol. 1151) (ed. B. D. Sleeman & R. J. Jarvis), pp. 304–316. New York: Springer.

Rinzel, J. 1987 A formal classification of bursting mechanisms in excitable systems. In *Proceedings of the International Congress of Mathematicians* (ed. A. M. Gleason), pp. 1578–1593. Rhode Island: American Mathematical Society.

Rinzel, J. & Lee, Y. S. 1986 On different mechanisms for membrane potential bursting. In *Nonlinear oscillations in biology and chemistry* (*Lecture notes in biomathematics* vol. 66), pp. 19–33. New York: Springer:

Rogawski, M. A. 1985 The A current: how ubiquitous a feature of excitable cells is it? *Trends Neurosci.* **8**, 214–219.

Rose, R. M. & Hindmarsh, J. L. 1985 A model of a thalamic neuron. *Proc. R. Soc. Lond.* B **225**, 161–193.

Rose, R. M. & Hindmarsh, J. L. 1989*a* The assembly of ionic currents in a thalamic neuron. II. The stability and state diagrams. *Proc. R. Soc. Lond.* B **237**, 389–312. (Following paper.)

Rose, R. M. & Hindmarsh, J. L. 1989*b* The assembly of ionic currents in a thalamic neuron. III. The seven-dimensional model. *Proc. R. Soc. Lond.* B. **237**, 313–334. (This volume.)

3

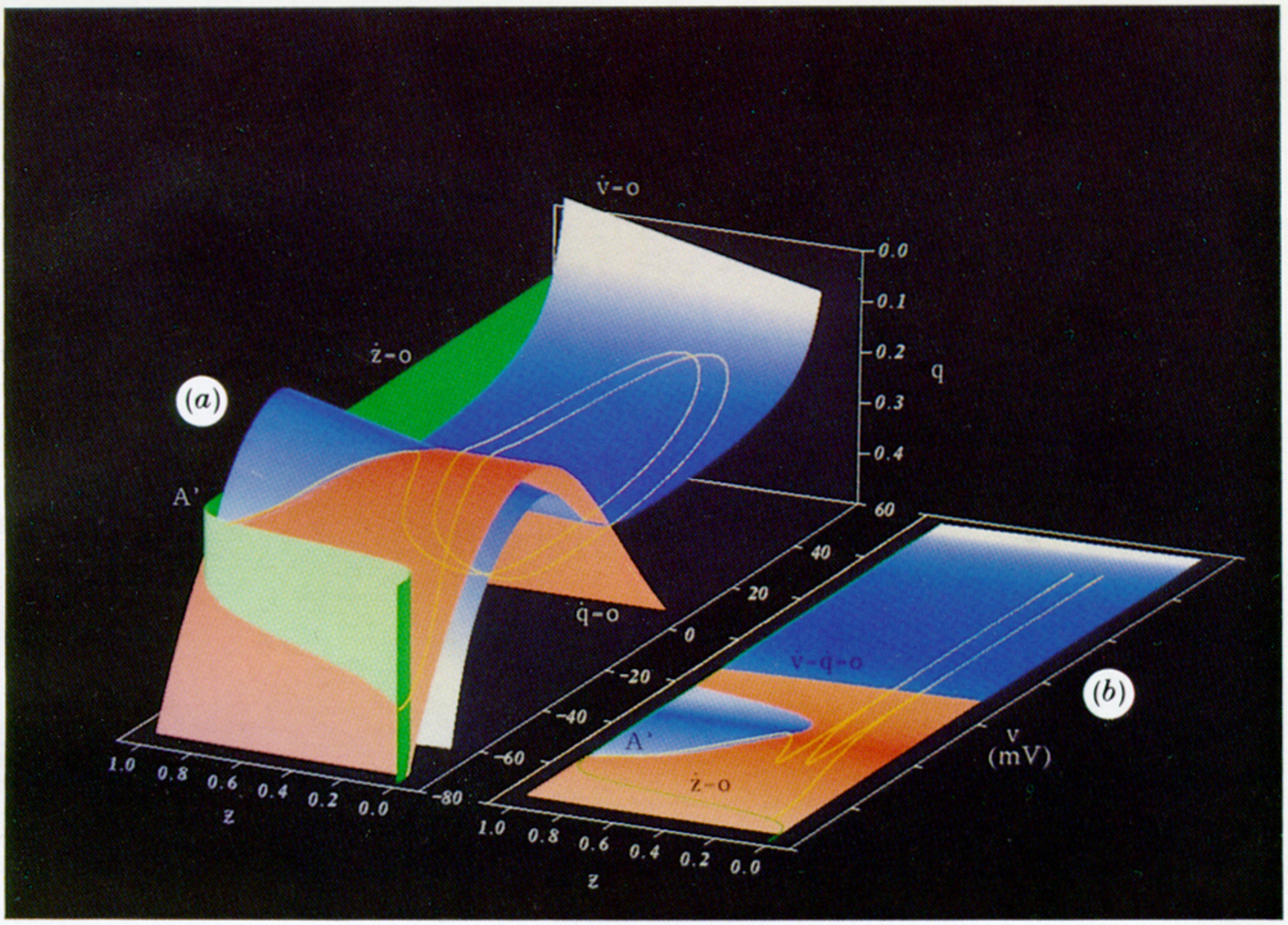

4

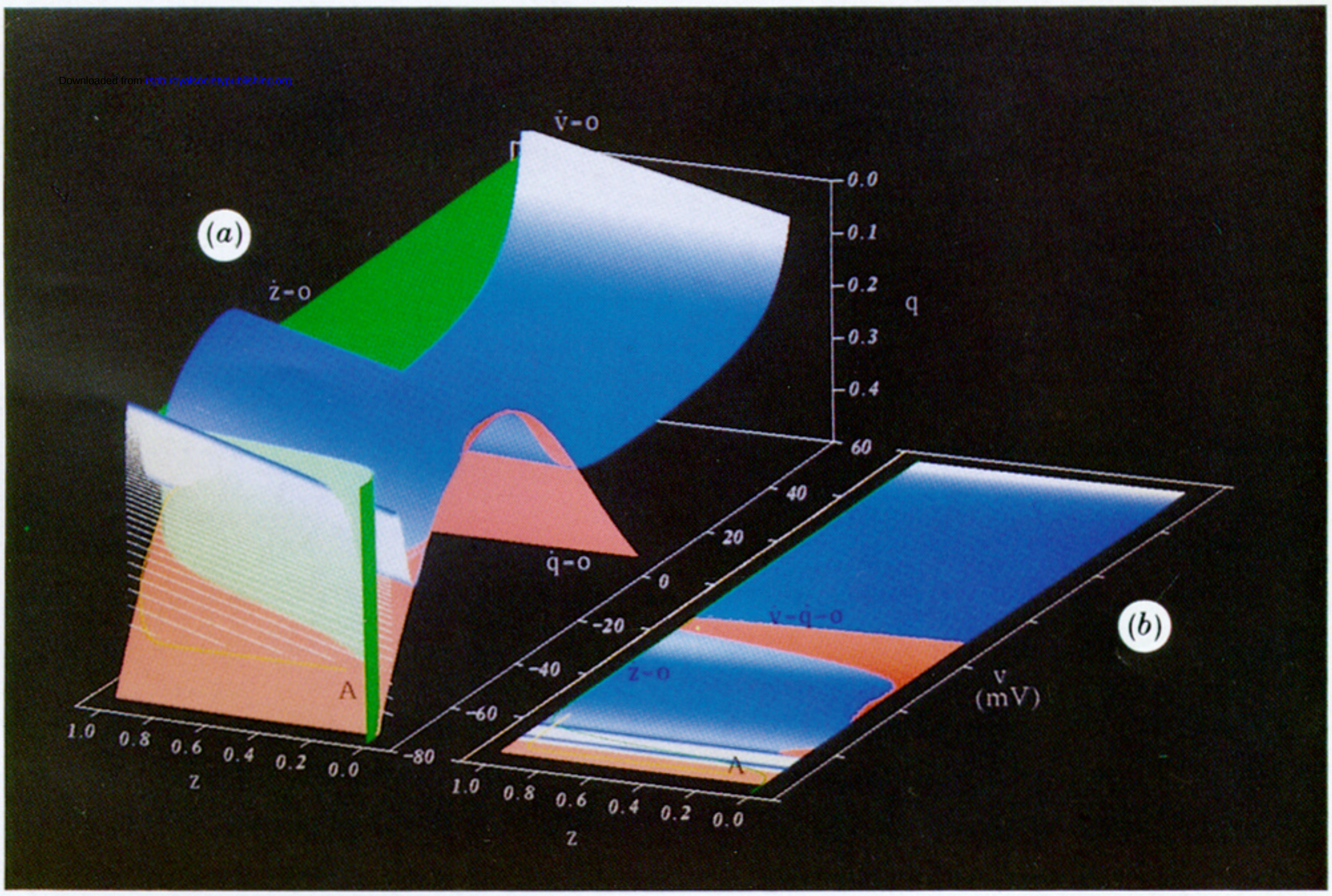

FIGURES 3 AND 4. For description see opposite.